

Skipper Charge-Coupled Device for Low-Energy-Threshold Particle Experiments above Ground

Guillermo Fernandez Moroni^{1,*}, Fernando Chierchie², Javier Tiffenberg¹, Ana Botti³,
Mariano Cababie^{3,1}, Gustavo Cancelo¹, Eliana L. Depaoli⁴, Juan Estrada¹, Stephen E. Holland⁵,
Dario Rodrigues^{3,1}, Iván Sidelnik⁶, Miguel Sofo Haro^{1,7}, Leandro Stefanazzi¹ and Sho Uemura⁸

¹*Fermi National Accelerator Laboratory, PO Box 500, Batavia, Illinois 60510, USA*

²*Instituto de Inv. en Ing. Eléctrica “Alfredo Desages” (IIIE), Dpto. de Ing. Eléctrica y de Computadoras.
CONICET and Universidad Nacional del Sur (UNS), Bahía Blanca, Argentina*

³*Department of Physics, FCEN, University of Buenos Aires and IFIBA, CONICET, Buenos Aires, Argentina*


⁴*CNEA - Gerencia de Área Aplicaciones de la Tecnología Nuclear (GAATN) - Gerencia Química Nuclear y Ciencias de la Salud - Dpto. Metrología de Radioisótopos - División Metrología Científica Centro Atómico Ezeiza, Ezeiza, Argentina*

⁵*Lawrence Berkeley National Laboratory, One Cyclotron Road, Berkeley, California 94720, USA*

⁶*CONICET y CNEA - Comisión Nacional de Energía Atómica, Departamento de física de neutrones,
Centro Atómico Bariloche, Av. Bustillo 9500, Bariloche, Argentina*

⁷*Centro Atómico Bariloche, CNEA/CONICET/IB, Bariloche, Argentina*

⁸*School of Physics and Astronomy, Tel-Aviv University, Tel-Aviv 69978, Israel*

 (Received 1 September 2021; revised 10 February 2022; accepted 1 March 2022; published 26 April 2022)

We present experimental results using a single-electron resolution skipper CCD running above ground level to demonstrate the potential of this technology for its use in reactor neutrino observations and other low-energy particle-interaction experiments. Operating conditions and event-selection criteria are provided to decouple most of the background rate at low energies. The majority of this background comes from interactions in the inactive silicon surrounding the active detector volume that ends up in the readout register of the sensor. Our final results are compared with other low-threshold technologies showing a good control of the background for low ionization energies down to five electron-hole pairs. This demonstrates that the skipper CCD proves to be among the best options to measure low-energy and weakly interacting particles at ground level.

DOI: [10.1103/PhysRevApplied.17.044050](https://doi.org/10.1103/PhysRevApplied.17.044050)

I. INTRODUCTION

Low-energy threshold particle experiments to research standard and beyond standard model interactions require two main characteristics: on one side, high-sensitivity sensors and at the same time, detailed control of the background levels of the experiment. Charge coupled devices (CCDs) silicon detectors with low readout noise and large active volume have been identified among the most promising technologies for the low-mass direct dark-matter search experiments, probing electron and nuclear recoils from sub-GeV mass [1–5]. In these kinds of physics searches, the background is highly reduced by operating the experiment deep underground reducing the cosmic rays' shower. The recent development of the skipper CCD [6–8] demonstrated the capability to measure ionization

events with subelectron noise extending the reach of this technology to unprecedented low energies. This enabled world-leading results for dark-matter searches at underground facilities [8]. Experiments based on this technology are planned for the coming years with active masses going from 100 g to several kilograms [9,10]. At the same time, the low-noise standard CCD technology has been implemented in a low-energy neutrino experiment [11,12]. This experiment runs above surface near the neutrino source, a nuclear reactor, thus losing the advantage of operating underground that dark-matter experiments have. Neutrino experiments with skipper CCDs are also being currently planned [13].

Rates of single-electron depositions larger than expected have been observed in Ref. [8], and its possible link to higher-energy particles has been summarized in Ref. [14]. Moreover, recent studies on regions in the CCD with low collection efficiency [15] show how large-energy ionization events could produce low-energy signals in

*gfmoroni@fnal.gov

the detector. For this reason, experiments running above ground are more challenging due to the larger rate of atmospheric high-energy particles [16].

In Ref. [17] it is shown that a good control of the background starting at around 15 up to 500 eV of ionization equivalent energy is a key factor for physics searches using neutrinos at nuclear reactors. Moreover, planned experiments for the study of silicon energy absorption from photon and neutron interactions, using skipper CCDs, require the detector at surface level to be operated with good control of the background. Several recent low-threshold technologies observe a rapidly increasing rate of background events towards low energies (below 1 keV). This effect is more evident when the detector is running above ground [18–26] compared to underground locations [8,27–29]. Larger background rates result in limiting the reach of the low-threshold capability of the sensor. The first edition of the EXCESS workshop in 2021 [30] exhibit the effort of the community to overcome this issue.

It is fairly known that the long readout time of the skipper-CCD sensors hinders the use of active veto systems and therefore is more susceptible to higher background contributions due to the cosmic ray interactions. For this reason, passive shield configurations together with event-selection criteria based on the spatial resolution of thick fully depleted CCDs are used to reject undesired signals. No previous study has addressed this problem for this sensor at surface level to achieve a controlled background at low energies.

In this paper we study the use of skipper CCDs as a potential low-threshold technology for experiments above surface. We start by presenting a case studying the detection of nuclear reactor neutrinos, to link the background at low energy with the significance for detection of the coherent elastic neutrino-nucleus scattering (CEvNS) interaction [31]. We then present the experimental setup and discuss the main sources of background found on the measurements. We propose a detector operation scheme and selection criteria to reject these contributions. We demonstrate that with the proposed technique, the low-energy excess in the background rate seen by other experiments [30] is not present using the skipper-CCD technology, even down to events producing an ionization of five electron-hole pairs. Finally, we compare the background measurements observed by other low-threshold technologies already published that have participated in the EXCESS workshop.

II. MOTIVATION: NUCLEAR-REACTOR NEUTRINO DETECTION

CEvNS is a particle interaction between a neutrino (or antineutrino) and the nucleus of the target atoms (in our case silicon) where the neutrino coherently scatters off

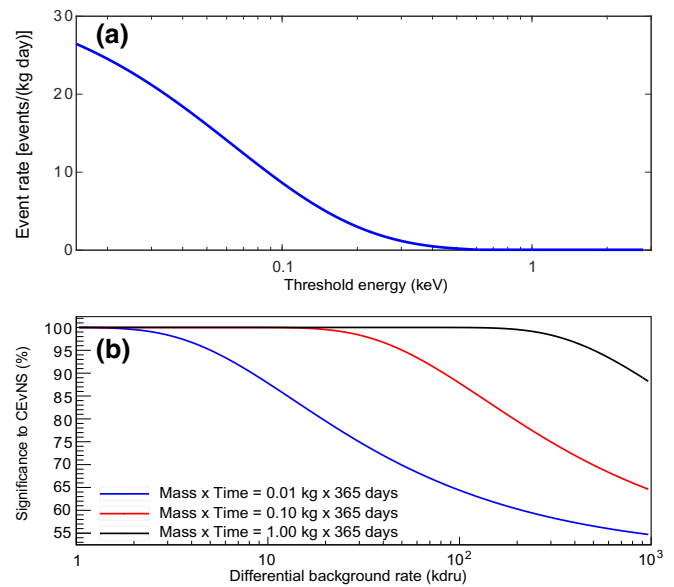


FIG. 1. (a) Expected number of neutrino events in silicon as a function of the energy threshold of the sensor; the energy unit is in ionization energy after quenching factor corrections. (b) Significance for detecting CEvNS as a function of the background level.

the whole nucleus instead of distinguishing its individual nucleons. The coherence of the interaction results in sensitivity to the square of the total weak charge of the nucleus, which could enhance the coherent scattering cross section by a factor 10–100 when compared to neutrino-nucleon scattering [32]. It takes place only for neutrino energies below approximately 50 MeV [31]. Power nuclear reactors provide the largest neutrino flux on the earth with energies up to approximately 12 MeV. This source provides the possibility to experimentally research standard and beyond standard physics in the neutrino sector. Nevertheless, measuring CEvNS interaction imposes challenges since very low energy is transferred to the nucleus and only a fraction of it (due to quenching factor) translates into observable ionization.

Figure 1(a) shows the number of expected events per kg of active mass per day as a function of the minimum observable ionization energy. The energy in the x axis is the amount of energy that goes into ionization (after quenching-factor correction). The quenching-factor parametrization in Ref. [12] (which is based on the measurements presented by Chavarria *et al.* [33]) is used for the calculations. In this plot and in all the results presented in this work the eV or keV units express electron equivalent energy (eVee or keVee) since the skipper sensors measure the ionized charge.

We consider an array of skipper-CCD silicon detectors located at 12 m from the center of the core of the Atucha

II Nuclear Power Plant with 2 GW of thermal power [13]. This is our target scenario for an experiment using skipper CCDs in close proximity of a power nuclear reactor [17,32]. Detailed explanation on how to compute the neutrino signal can be obtained from Refs. [32,34]. As seen in Fig. 1(a) most of the measurable events are expected to produce 100 eV of ionization energy or less with the rate reaching almost zero above 300 eV. Sensor technologies should have an energy threshold below 300 eV to access a big fraction of the reactor neutrino flux. However, the benefits from reducing the energy threshold must be accompanied by a well control of the background event rate. The neutrino signal grows towards lower energies, if the background spectrum has a similar behavior, then any systematic error in its estimation could limit the sensitivity of the observation because the residual background could mimic the expected signal. Unfortunately there is little published information of the background for experiments above ground for energies below 1 keV. Moreover, as we discuss later, other technologies have evidenced a large increase of the background rate towards low energies [30].

Figure 1(b) shows the significance to observe CEvNS signal as a function of the differential background level [in $\text{kdr} = 1000 \text{ events}/(\text{day kg keV})$] using skipper CCDs for different experiment scenarios: total sensor active mass of 0.01, 0.1, and 1 kg running for 365 days of observation. Significance is calculated assuming a known background model by comparing the total rate of a neutrino signal in the energy interval 15 to 100 eV to the statistical fluctuation of the background rate on the same range. No systematic errors are assumed. The lowest energy limit is adopted from Ref. [17,32] as a conservative minimum energy to prevent on-chip noise sources. The maximum limit is chosen to maximize the signal-to-noise ratio. The results in Fig. 1(b) show that background rates between a few kdr and below 100 kdr provide good scenarios to get high detection confidence levels in one year for experimental setups with a few hundreds grams of active mass. Current research and development in skipper-CCD and readout technology [35] and the experience on integrating many CCDs on a single array [8,12,29] allows such setups to be built.

This case reveals the relevance of controlling the background for detecting CEvNS from nuclear reactor neutrinos, especially in the low-energy region below 300 eV. Despite background rates as large as 100 kdr can be handled using large mass experiments, the scientific reach of neutrino observation is significantly improved from smaller background rates [32]. Towards low energies most experiments show a fast regrowth of the background level. Next, experimental results and background reduction techniques are presented using a skipper-CCD sensor to achieve a reduced background level in this low-energy range.

III. DESCRIPTION OF THE EXPERIMENT

Figure 2(a) shows the experimental setup where some of the main components are labeled. One skipper CCD [shown in Fig. 2(b)] is operated at a temperature of 140 K using a Sunpower cryocooler [36]. The CCD is glued to a silicon substrate that sits on a copper tray for mechanical support as well as thermal connectivity. The CCD is placed in an extension of the dewar that fits inside a lead cylinder. A lead cap on top of the sensor (inside the dewar extension) completes the lead shield of 2 in. of thickness around the device. There is no radio purity selection of materials inside the shield. The CCD was designed by the LBNL Microsystems Laboratory (MSL) [37] and fabricated at Teledyne-DALSA. It has 6144 columns by 1024 rows with pixels of $15 \times 15 \mu\text{m}^2$ with a thickness of $675 \mu\text{m}$, giving a total active mass of 2.2 g. It is read by four amplifiers, one on each corner, using a low-threshold acquisition (LTA) controller [35]. Two quadrants present larger readout noise and are not used for the analysis in the following sections. The sensor is operated at subelectron noise by averaging 300 measurements of the charge in each pixel [7] and with a horizontal binning [38] of ten columns.

Two different kinds of measurements are performed:

(a) Dataset A: Interactions in the active region. 3.21 days of data are collected from the active region of the sensor in continuous readout mode [8].

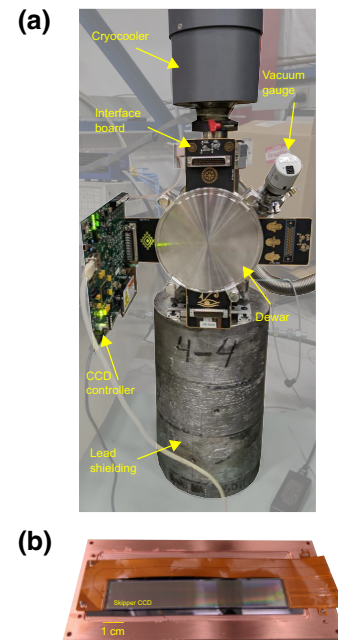


FIG. 2. (a) Setup used for the experiment with a short description of the main components. (b) A picture of the CCD installed on the copper tray. An extra copper plate that covers the top part of the sensor is not presented in the image.

(b) Dataset B: Interactions collected in the serial register (also called horizontal register). It consists of charge packets collected only by the serial register, not coming from the active region, from here on called “serial-register events” [39]. To make an isolated measurement of this source of events, the vertical lines of the sensor are left in idle mode while clocking only the control signals from the serial and output stage. In other words, the sensor is read out as in dataset A but without moving the charge from the active area to the serial register. 2.7 days are collected in this mode.

IV. DETECTOR CALIBRATION AND NOISE SOURCES

An absolute energy calibration of the sensor is performed using the electron counting capability. A histogram of the pixel values from the active region (dataset A) is produced as shown in Fig. 3, each peak correspond to an integer number of electrons in the pixel. The peaks are fitted using a Gaussian distribution whose mean value is used to build a look-up table (digital unit versus electrons) to calibrate the sensor up to around $700 e^-$. Following the convention in Ref. [32], for the calibration between ionized charge q in electrons to energy we use 3.75 eVee as the average energy deposition per collected electron [40]. To make the selection cut for events with $5 e^-$ of charge or more and taking into account the Gaussian readout noise observed around each peak in Fig. 3, events starting at 16.87 eV ($4.5 e^-$) are considered for the analysis. The single-pixel x-ray events with energy of 8.048 keV produced by the fluorescence of the surrounding copper material correspond to $2146 e^-$ ionized electrons. The readout noise of the sensor, evaluated as the standard deviation of the values of the empty pixels ($0 e^-$ peak in Fig. 3), is $0.165 e^-$ and $0.167 e^-$ for the two quadrants in use. The average single-electron rates per pixel measured are $0.01 e^-/\text{pix}$ and $0.009 e^-/\text{pix}$ after binning in each quadrant, with a contribution from the exposure-dependent charge production [41] of $0.018 e^-/(\text{pix day})$ (pixels before binning). The diffusion charge transport of carriers in the bulk of the sensor is measured and it turns out to be similar to that previously published in Ref. [8].

V. STUDY OF THE EXTRACTED INTERACTION

A clustering algorithm is applied to the images to extract events produced by particle interactions. Figure 4 shows the shape and energy distributions of the analyzed events. Left plots show the event size in the y direction (rows of the image), σ_y (determined as the standard deviation of the charge distribution in the pixels of the event) as a function of energy for three different datasets: the two previously discussed and a third set generated from a simulation. The plots on the right show the relationship between the size (σ_x) in x direction (columns of the image) and σ_y .

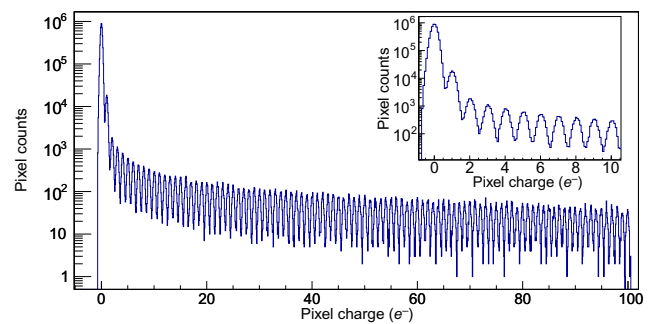


FIG. 3. Histogram of pixels with charge up to $100 e^-$ after calibration. Single-electron discrimination is observed. The inset shows the same histogram for the first ten peaks.

Figures 4(a) and 4(b) correspond to simulations of particle energy depositions in the active region (bulk) of the sensor. The software places charge packets in the bulk of the silicon and simulates the transport due to drift and diffusion of these free carriers until they are trapped by the potential well of the pixels. The simulation technique is based on previous studies in Ref. [42]. 30 000 events are simulated with ionization uniformly distributed from 5 to 800 electron-hole pairs. The transport of the carriers uses the measured diffusion in the sensor from Ref. [8]. The only particles that are able to produce low-energy interaction (below 3 keV of deposited energy) deep in the bulk (several micrometers away from the front and back surfaces of the sensor) are from Gammas and neutron through Compton and nuclear scattering, respectively. These particles have a mean free path in silicon much larger than the detector size, so the ionizations are expected to be uniformly distributed in its volume as used for the simulated events. Since the charge of ten columns is collapsed into one, due to the horizontal binning, there is little information left concerning the shape of the event in the x direction of the output images as shown in Fig. 4(b). Some events present $\sigma_x > 0$. They take place on the edge of the binned regions and have information shared between two binned pixels and their probability of occurrence is low.

From Fig. 4(a) we can see that the σ_y distribution is similar for all energies. Most of the events have a σ_y larger than 0.4 pixels (see color scale) with a maximum of about 1.1 pixels due to the maximum expected lateral diffusion.

Figures 4(c) and 4(d) show the distribution of events measured in the serial register (dataset B). For this measurement the content of the active area of the CCD is not transferred to the serial register. Any event that directly interacts with this serial register, either because it occurs therein or from an event in the inactive silicon surrounding the active detector volume that end up collected directly by the serial register, will be seen as a single-row interaction in the final image. Because of this, serial-register events have practically no spatial information in the y

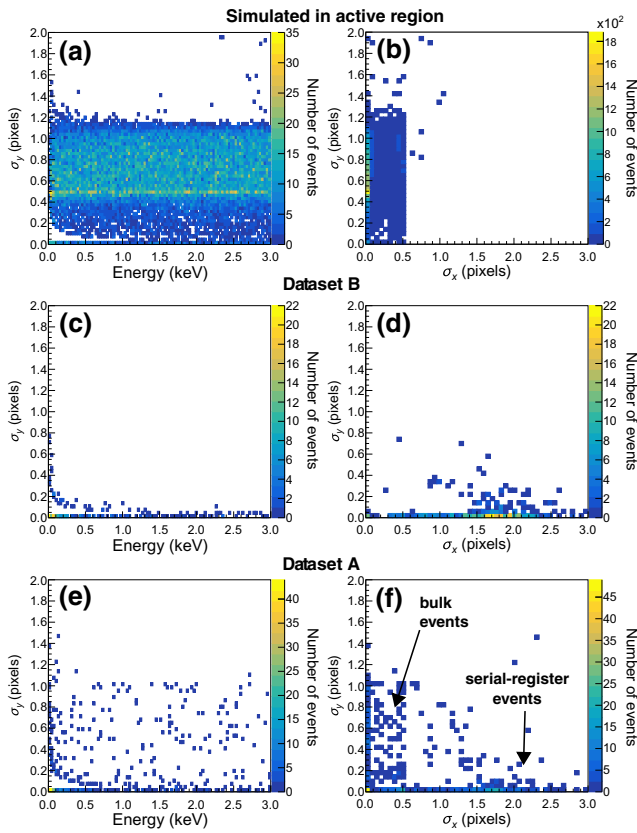


FIG. 4. Morphology of the events in the output image: (a),(b) are the expected events from true interactions in the sensor generated from simulations; (c),(d) serial-register event contributions measured without dumping the collected charge in the active volume to the serial register; and (e),(f) measured events in the active region of the sensor.

direction (σ_y distribution close to 0) and extend mostly on the x direction populating the σ_x axis for values larger than zero. The spread of the σ_x distribution is wider than for the events in the bulk [compare Figs. 4(b) and 4(d)] since they occur in the undepleted silicon (with no electric field) so the charge can diffuse more before it is collected by the serial register pixels. A dark-current signal following a Poisson distribution with mean equal to $0.01 e^-/\text{pixel}$ (after binning, as measured in dataset A) is added to the pixels in the output data to emulate both contributions together. Low-energy events may appear with an increased size in the y direction due to dark counts in neighboring rows paired in the same cluster.

The third group in Figs. 4(e) and 4(f) corresponds to measurements in the active region of the sensor (dataset A). The plots show components of the previously mentioned contribution: (1) events from the bulk (as in the simulations) and (2) from the serial register. The first have sizes below 1.1 pixels in y direction and smaller than 0.5 pixel in x direction, as expected from the charge-transport

calibration and event simulations, while the second populates both plots for small σ_y .

Serial register events are not observed before using standard CCD and total readout time of a few minutes [11] after an exposure of a few hours. The extra readout time of the skipper CCD requires longer time using the serial register and therefore more chances to grab these events. The proposed horizontal binning also accelerates the total readout time of the serial register, and thus it reduces the exposure time to this source of spurious events. As shown in the previous analysis, it also provides the advantage of orthogonalization of the size information for both sources of events, and therefore a purer selection of bulk events can be made.

In the following section we use a combination of constraints on both σ_x and σ_y to separate the bulk events from the serial-register events in dataset A.

VI. EVENT SELECTION, FINAL SPECTRUM, AND COMPARISON WITH OTHER TECHNOLOGIES

Figure 5(a) shows the measured differential spectra of events in the active region with five or more electrons of ionized charge (from dataset A). Columns of the CCD that presented high single-electron rate (hot columns [38]) are eliminated from the analysis at an early stage. The remaining active mass of the sensor in use is 0.675 g (from the total 2.2 g, and after discarding two quadrants due to higher noise). The gray plot depicts all events reconstructed from the output images showing an increase of the rate towards low energy. The peak at around 8 keV corresponds to the fluorescence x rays from the copper in the mechanical package of the sensor. To study the impact of the results obtained in the previous section a selection criteria based on the event shape is performed. Figure 6 shows the one-dimensional distribution of the size, in x and y directions, for the events simulated in the active region of the sensor. Although events in the bulk can show a size in σ_x up to 0.5 pixels [Fig. 6(b)], the majority of them (72%) have a width smaller than 0.1 pixels.

A constraint of $\sigma_x < 0.3$ is used to provide strong rejection to the serial-register and dark-current events. At the same time, only sizes in the y direction compatible with depositions in the bulk are selected: $0.3 < \sigma_y < 1$, with the minimum limit chosen to prevent counting serial-register events. The spectrum of events after the selection cuts is also shown in blue in Fig. 5(a). Most of the low-energy excess is removed because its contribution is coming from the serial register. The average flux of events below 7.5 keV of energy is 12 kdr. The spectrum is normalized by the active mass of the sensor, but not by the efficiency of the selection criteria.

The inset focuses in energies below 200 eV. Although statistical errors do not allow the shape of the spectrum

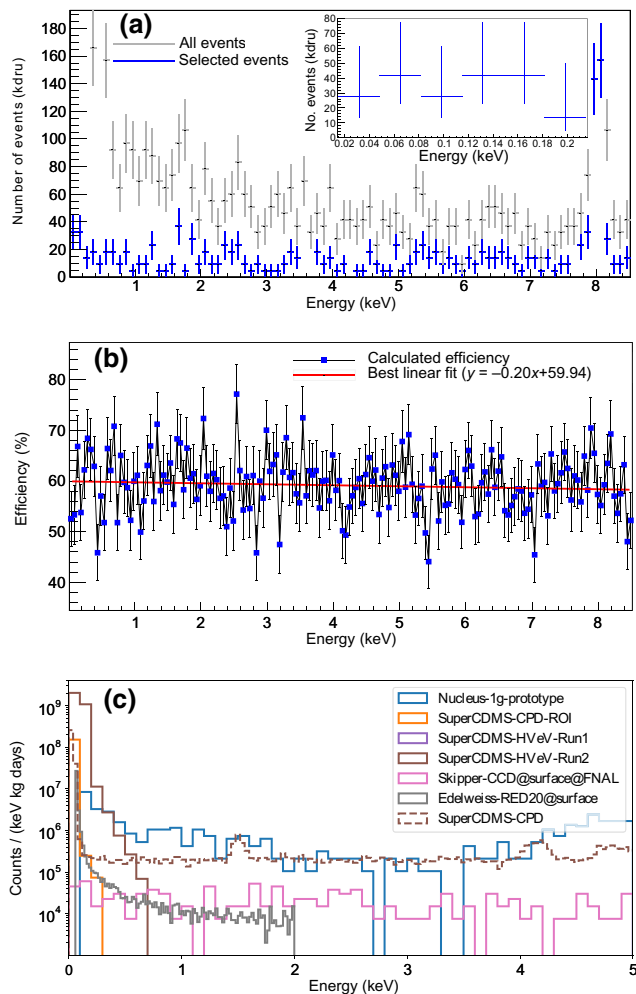


FIG. 5. (a) Energy spectrum before and after applying the selection criteria to the data (not weighted by the selection efficiency). The first two bins of the spectrum for all the events exceeds the selected maximum value in the y axes. The inset shows the distribution of the selected events with thinner bins at low energy. The error bar in the inset is chosen to have a symmetric coverage probability of 68.25% around the mean value. (b) Efficiency of the selection cuts. (c) Comparison of our results (Skipper-CCD@surface@FNAL) with other low-energy technologies presented in Ref. [30].

with energy to be mathematically modeled, a rapid growth of the spectrum at low energy is not observed.

Using the results for the bins between 15 and 100 eV in the inset of Fig. 5(a) and the average 60% efficiency shown in Fig. 5(b) a background of approximately 54 kdr is achieved. Based on the analysis presented in Sec. II and specifically in Fig. 1(b), having this background level and 100 g active sensor would result in a significance to observe CEvNS of around 95% during one year of observation of neutrinos from a nuclear reactor. This is just a preliminary result since lead thickness of the shield and radio purity of the materials are not optimized for these

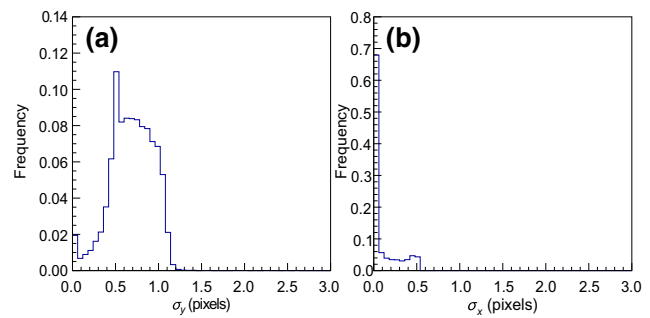


FIG. 6. Size distribution of events simulated in the active region of the sensor: (a) in the y axis, (b) in the x axis. The bins are normalized by the total number of simulated events.

measurements. We expect to improve the overall background level with a better design of the passive shield and its components, an approach similar to the work done for the CONNIE experiment using nonskipper CCDs [11].

To evaluate the efficiency of the selection criteria, simulated events from interactions spatially and energetically uniformly distributed in the active volume of the sensor are added to the real images. The diffusion transport model of carriers are also used in this simulation. The percentage of reconstructed events passing the selection criteria is shown in Fig. 5(b). Each energy bin is 50 eV wide and the first bin starts at 15 eV. The efficiency is almost flat for all energies showing that the final shape of the spectra is not modified by the selection criteria. The red curve shows a linear fit of the points, which can be used to normalize the spectra in Fig. 5(a) by the efficiency of the selection criteria

The results in this work compared to other current technologies for low-threshold experiment are shown in Fig. 5(c). The plot is produced using the online tool provided by organizers of the EXCESS workshop [30]. Only datasets from measurements above ground with published results are compared in the plot. Table I summarizes the references to the articles where the detector and data-analysis information is presented. All spectra are normalized by efficiency. Our results do not show the rapidly increasing rate of events observed for the other technologies for energies below 1 keV. There are other technologies

TABLE I. References for the plot spectra shown in Fig. 5(c). References obtained from Ref. [30].

Legend in Fig. 5(c)	References
Skipper-CCD@surface@FNAL	This paper
Nucleus-1g-prototype	[18–21]
SuperCDMS-CPD-ROI	[22]
SuperCDMS-HVeV-Run1	[23]
SuperCDMS-HVeV-Run2	[24]
Edelweiss-RED20@surface	[25]
SuperCDMS-CPD	[26]

that did not participate in the EXCESS workshop and are being developed to detect reactor neutrinos such as those using Germanium crystals [43,44]. Those experiments show very low background levels but their energy thresholds are between 200 and 300 eV, an order of magnitude larger than the threshold in this work.

VII. CONCLUSIONS

Experimental results using a single-electron resolution skipper CCD running above ground have been presented. We demonstrated the potential of this technology for reactor neutrinos and other low-energy particle-interaction experiments. A background source of events specially affecting the skipper CCD has been identified and a technique to decouple its contribution is presented. Our final result for events with energies of five ionized electron-hole pairs or more was compared to other state-of-the-art low-energy-threshold technologies showing a reduced background-increasing rate towards lower energies.

ACKNOWLEDGMENTS

We thank the SiDet team at Fermilab for the support on the construction and operation of skipper-CCD setups, especially Kevin Kuk and Andrew Lathrop. This work is supported by Fermilab under DOE Contract No. DE-AC02-07CH11359. This manuscript has been authored by Fermi Research Alliance, LLC under Contract No. DE-AC02-07CH11359 with the U.S. Department of Energy, Office of Science, Office of High Energy Physics. The CCD development work is supported in part by the Director, Office of Science, of the U.S. Department of Energy under No. DE-AC02-05CH11231. The U.S. Government retains and the publisher, by accepting the article for publication, acknowledges that the U.S. Government retains a nonexclusive, paid-up, irrevocable, worldwide license to publish or reproduce the published form of this manuscript, or allow others to do so, for U.S. Government purposes.

-
- [1] A. Aguilar-Arevalo *et al.*, (DAMIC), Search for low-mass WIMPs in a 0.6 kg day exposure of the DAMIC experiment at SNOLAB, *Phys. Rev. D* **94**, 082006 (2016).
- [2] A. Aguilar-Arevalo *et al.*, (DAMIC), First Direct-Detection Constraints on eV-Scale Hidden-Photon Dark Matter with DAMIC at SNOLAB, *Phys. Rev. Lett.* **118**, 141803 (2017).
- [3] A. Aguilar-Arevalo *et al.*, (DAMIC), Constraints on Light Dark Matter Particles Interacting with Electrons from DAMIC at SNOLAB, *Phys. Rev. Lett.* **123**, 181802 (2019).
- [4] M. Crisler, R. Essig, J. Estrada, G. Fernandez, J. Tiffenberg, M. Sofo haro, T. Volansky, and T.-T. Yu, (SENSEI), SENSEI: First Direct-Detection Constraints on sub-GeV Dark Matter from a Surface Run, *Phys. Rev. Lett.* **121**, 061803 (2018).
- [5] O. Abramoff *et al.*, (SENSEI), SENSEI: Direct-Detection Constraints on Sub-GeV Dark Matter from a Shallow Underground Run Using a Prototype Skipper-CCD, *Phys. Rev. Lett.* **122**, 161801 (2019).
- [6] G. Fernandez Moroni, J. Estrada, G. Cancelo, S. Holland, E. Paolini, and H. Diehl, Sub-electron readout noise in a skipper ccd fabricated on high resistivity silicon, *Exp. Astron.* **34**, 43 (2012).
- [7] J. Tiffenberg, M. Sofo-Haro, A. Drlica-Wagner, R. Essig, Y. Guardincerri, S. Holland, T. Volansky, and T.-T. Yu, Single-Electron and Single-Photon Sensitivity with a Silicon Skipper CCD, *Phys. Rev. Lett.* **119**, 131802 (2017).
- [8] L. Barak, I. M. Bloch, M. Cababie, G. Cancelo, L. Chaplinsky, F. Chierchie, M. Crisler, A. Drlica-Wagner, R. Essig, and J. Estrada *et al.*, SENSEI: Direct-Detection Results on sub-GeV Dark Matter from a New Skipper-CCD, arXiv e-prints, arXiv:2004.11378 (2020).
- [9] M. Settimo, Search for low-mass dark matter with the DAMIC experiment, arXiv e-prints, arXiv:2003.09497 (2020).
- [10] A. Aguilar-Arevalo, F. A. Bessia, N. Avalos, D. Baxter, X. Bertou, C. Bonifazi, A. Botti, M. Cababie, G. Cancelo, and B. A. Cervantes-Vergara *et al.*, The oscura experiment, arXiv preprint arXiv:2202.10518 (2022).
- [11] A. Aguilar-Arevalo, X. Bertou, C. Bonifazi, G. Cancelo, A. Castañeda, B. Cervantes Vergara, C. Chavez, J. C. D’Olivo, J. C. Dos Anjos, and J. Estrada *et al.*, (CONNIE Collaboration), Exploring low-energy neutrino physics with the coherent neutrino nucleus interaction experiment, *Phys. Rev. D* **100**, 092005 (2019).
- [12] A. Aguilar-Arevalo, X. Bertou, C. Bonifazi, G. Cancelo, B. A. Cervantes-Vergara, C. Chavez, J. C. D’Olivo, J. C. Dos Anjos, and J. Estrada *et al.*, CONNIE Collaboration, Search for light mediators in the low-energy data of the CONNIE reactor neutrino experiment, *J. High Energy Phys.* **2020**, 54 (2020).
- [13] J. D’Olivo, C. Bonifazi, D. Rodrigues, and G. F. Moroni, *νIOLETA*: neutrino interaction observation with a low energy threshold array, *XXIX Int. Conf. Neutrino Phys.* (2020).
- [14] P. Du, D. Egana-Ugrinovic, R. Essig, and M. Sholapurkar, Sources of low-energy events in low-threshold dark matter detectors, arXiv:2011.13939 [hep-ph] (2020).
- [15] G. F. Moroni, K. Andersson, A. Botti, J. Estrada, D. Rodrigues, and J. Tiffenberg, Charge-Collection Efficiency in Back-Illuminated Charge-Coupled Devices, *Phys. Rev. Appl.* **15**, 064026 (2021).
- [16] T. K. Gaisser, R. Engel, and E. Resconi, *Cosmic Rays and Particle Physics* (Cambridge University Press, Cambridge, England, 2016).
- [17] G. Fernandez-Moroni, P. A. Machado, I. Martinez-Soler, Y. F. Perez-Gonzalez, D. Rodrigues, and S. Rosauero-Alcaraz, The physics potential of a reactor neutrino experiment with skipper ccds: Measuring the weak mixing angle, *J. High Energy Phys.* **2021**, 1 (2021).
- [18] R. Strauss, J. Rothe, G. Angloher, A. Bento, A. Gütlein, D. Hauff, H. Kluck, M. Mancuso, L. Oberauer, and F. Petricca *et al.*, Gram-scale cryogenic calorimeters for rare-event searches, *Phys. Rev. D* **96**, 022009 (2017).
- [19] G. Angloher, P. Bauer, A. Bento, C. Bucci, L. Canonica, X. Defay, A. Erb, F. v. Feilitzsch, N. F. Iachellini, and P. Gorla

- et al.*, Results on meV-scale dark matter from a gram-scale cryogenic calorimeter operated above ground, *Eur. Phys. J. C* **77**, 637 (2017).
- [20] B. Flebus, G. E. W. Bauer, R. A. Duine, and Y. Tserkovnyak, Theory of the magnon-mediated tunnel magneto-seebeck effect, *Phys. Rev. B* **96**, 094429 (2017).
- [21] J. Rothe, G. Angloher, F. Ardellier-Desages, A. Bento, L. Canonica, A. Erhart, N. Ferreiro, M. Friedl, V. M. Ghete, and D. Hauff *et al.*, Nucleus: Exploring coherent neutrino-nucleus scattering with cryogenic detectors, *J. Low Temp. Phys.* **199**, 433 (2020).
- [22] C. W. Fink, S. L. Watkins, T. Aramaki, P. L. Brink, J. Camilleri, X. Defay, S. Ganjam, Y. G. Kolomensky, R. Mahapatra, and N. Mirabolfathi *et al.*, Performance of a large area photon detector for rare event search applications, *Appl. Phys. Lett.* **118**, 022601 (2021).
- [23] R. Agnese, T. Aralis, T. Aramaki, I. J. Arnquist, E. Azadbakht, W. Baker, S. Banik, D. Barker, D. A. Bauer, and T. Binder *et al.*, First Dark Matter Constraints from a Supercdms Single-Charge Sensitive Detector, *Phys. Rev. Lett.* **121**, 051301 (2018).
- [24] D. W. Amaral, T. Aralis, T. Aramaki, I. J. Arnquist, E. Azadbakht, S. Banik, D. Barker, C. Bathurst, D. A. Bauer, and L. V. S. Bezerra *et al.*, Constraints on low-mass, relic dark matter candidates from a surface-operated supercdms single-charge sensitive detector, *Phys. Rev. D* **102**, 091101 (2020).
- [25] E. Armengaud *et al.*, (EDELWEISS), Searching for low-mass dark matter particles with a massive ge bolometer operated above ground, *Phys. Rev. D* **99**, 082003 (2019).
- [26] I. Alkhatib, D. W. P. Amaral, T. Aralis, T. Aramaki, I. J. Arnquist, I. A. Langroudy, E. Azadbakht, S. Banik, D. Barker, and C. Bathurst *et al.*, Light dark matter search with a high-resolution athermal phonon detector operated above ground, [arXiv:2007.14289](https://arxiv.org/abs/2007.14289) [hep-ex] (2021).
- [27] A. H. Abdelhameed, G. Angloher, P. Bauer, A. Bento, E. Bertoldo, C. Bucci, L. Canonica, A. D’Addabbo, X. Defay, and S. Di Lorenzo *et al.*, (CRESST Collaboration), First results from the CRESST-III low-mass dark matter program, *Phys. Rev. D* **100**, 102002 (2019).
- [28] C. Collaboration, A. H. Abdelhameed, G. Angloher, P. Bauer, A. Bento, E. Bertoldo, C. Bucci, L. Canonica, A. D’Addabbo, and X. Defay *et al.*, Description of CRESST-III data, [arXiv:1905.07335](https://arxiv.org/abs/1905.07335) [astro-ph.CO] (2020).
- [29] A. Aguilar-Arevalo, D. Amidei, D. Baxter, G. Canelo, B. A. C. Vergara, A. E. Chavarria, J. C. D’Olivo, J. Estrada, F. Favela-Perez, and R. Gaïor *et al.*, (DAMIC Collaboration), Results on Low-Mass Weakly Interacting Massive Particles from an 11 kg d Target Exposure of Damic at Snolab, *Phys. Rev. Lett.* **125**, 241803 (2020).
- [30] E. Workshop, “Data repository,” (2021).
- [31] D. Z. Freedman, Coherent effects of a weak neutral current, *Phys. Rev. D* **9**, 1389 (1974).
- [32] G. Fernandez-Moroni, R. Harnik, P. Machado, I. Martinez-Soler, Y. Perez-Gonzalez, D. Rodrigues, and S. Rosauro-Alcaraz, The physics potential of a reactor neutrino experiment with skipper-ccds: Searching for new physics with light mediators, [arXiv preprint arXiv:2108.07310](https://arxiv.org/abs/2108.07310) (2021).
- [33] A. Chavarria *et al.*, Measurement of the ionization produced by sub-keV silicon nuclear recoils in a CCD dark matter detector, *Phys. Rev. D* **94**, 082007 (2016).
- [34] G. Fernandez Moroni, J. Estrada, E. E. Paolini, G. Canelo, J. Tiffenberg, and J. Molina, Charge coupled devices for detection of coherent neutrino-nucleus scattering, *Phys. Rev. D* **91**, 072001 (2015).
- [35] G. I. Canelo, C. Chavez, F. Chierchie, J. Estrada, G. Fernandez-Moroni, E. E. Paolini, M. S. Haro, A. Soto, L. Stefanazzi, and J. Tiffenberg *et al.*, Low threshold acquisition controller for skipper charge-coupled devices, *J. Astron. Telesc. Instrum. Syst.* **7**, 1 (2021).
- [36] Sunpower cyocoolers.
- [37] Lawrence Berkeley National Laboratory (LBNL), <https://engineering.lbl.gov/microsystems-laboratory/>.
- [38] J. R. Janesick, *Scientific Charge-Coupled Devices* (SPIE press, Bellingham, Washington, USA, 2001), Vol. 83.
- [39] Later it will be shown that these depositions dominate the low-energy spectrum in the output data. This charge is generated in the inactive silicon surrounding the active volume on the edges of the die. The charge can diffuse from the undepleted region and eventually reach the collection region of the pixels in the serial register. For more information about the sensor electrostatic see Ref. [45].
- [40] D. Rodrigues, K. Andersson, M. Cababie, A. Donadon, A. Botti, G. Canelo, J. Estrada, G. Fernandez-Moroni, R. Piegaia, and M. Senger *et al.*, Absolute measurement of the fano factor using a skipper-ccd, *Nucl. Instrum. Methods Phys. Res. Section A: Accelerators, Spectrometers, Detectors Associated Equipment* **1010**, 165511 (2021).
- [41] L. Barak, I. M. Bloch, A. Botti, M. Cababie, G. Canelo, L. Chaplinsky, F. Chierchie, M. Crisler, A. Drlica-Wagner, and R. Essig *et al.*, Sensei: Characterization of single-electron events using a skipper-CCD, [arXiv:2106.08347](https://arxiv.org/abs/2106.08347) [physics.ins-det] (2021).
- [42] M. S. Haro, G. Fernandez Moroni, and J. Tiffenberg, Studies on small charge packet transport in high-resistivity fully depleted ccds, *IEEE Trans. Electron Devices* **67**, 1993 (2020).
- [43] H. Bonet, A. Bonhomme, C. Buck, K. Fülber, J. Hakenmüller, J. Hempfling, G. Heusser, T. Hugle, M. Lindner, and W. Maneschg *et al.*, Full background decomposition of the conus experiment, [arXiv:2112.09585](https://arxiv.org/abs/2112.09585) [physics.ins-det] (2021).
- [44] J. Colaresi, J. I. Collar, T. W. Hossbach, A. R. L. Kavner, C. M. Lewis, A. E. Robinson, and K. M. Yocum, First results from a search for coherent elastic neutrino-nucleus scattering at a reactor site, *Phys. Rev. D* **104**, 072003 (2021).
- [45] S. E. Holland, D. E. Groom, N. P. Palaio, R. J. Stover, and M. Wei, Fully depleted, back-illuminated charge-coupled devices fabricated on high-resistivity silicon, *IEEE Trans. Electron Devices* **50**, 225 (2003).